The California Land-falling Jets Experiment CALJET: Motivation, Strategy, and Description of a Flooding Event

Dr. F. Martin Ralph

NOAA/ERL/Environmental Technology Laboratory, Boulder, CO

The initial objectives of the CALJET experiment were to explore the role of coastal and offshore observations of low-level jets (LLJ) and their mesoscale environment in land-falling winter storms on mesoscale quantitative precipitation and wind forecasting. New goals were added when the strong El Niño of 1997/98 developed and it became evident that there was a substantially increased risk of flooding in California.

The experiment focused on the LLJ because it plays a key role in determining coastal orographic rainfall. Although orographic rainfall is very sensitive to the speed, orientation, and moisture content of the low-level flow as it encounters the coastal mountains, these parameters are poorly known even shortly before a storm makes land fall.

This presentation will describe the motivation for the experiment and the associated observing strategy. Preliminary results will be illustrated by describing an event where up to 12 inches of rain fell 24 h along the Big Sur Coast in central California. The evolution of this event over 48 h, including the incipient stage as the storm developed offshore and the devastating rainfall and flooding it caused upon land fall, will be examined.

Reprints of three recent conference papers presented at the Annual Meeting of the American Meteorological Society in Dallas, Texas during January 1999 are appended here. They provide more background on the experiment and a summary of the field phase (Ralph et al.), as well as analyses of a two strong storms on 2-3 February 1998 (Persson et al.) and on 5-6 February 1998 (White et al.).

Preprints, 3rd Symposium on Integrated Observing Systems, Dallas, TX, Amer. Meteor. Soc., p. 78-81.

8.1 THE CALIFORNIA LAND-FALLING JETS EXPERIMENT (CALJET): OBJECTIVES AND DESIGN OF A COASTAL ATMOSPHERE-OCEAN OBSERVING SYSTEM DEPLOYED DURING A STRONG EL NIÑO

F. M. Ralph*[1], P. O. G. Persson[2], D. Reynolds[3], W. Nuss[4], D. Miller[4], J. Schmidt[5], D. Jorgensen [6], J. Wilczak[1], P. Neiman[1], J.-W. Bao[2], D. Kingsmill[7], Z. Toth[8], C. Veldon[9], A. White[2], C. King[1], and J. Wurman[10]

[1]NOAA/ERL/Environmental Technology Laboratory, Boulder, CO; [2]CIRES/NOAA, Univ. of Colorado, Boulder, CO; [3]NOAA/NWS/Hydrometeorological Prediction Center, Washington, DC; [4]Naval Postgraduate School, Monterey, CA [5]Naval Research Laboratory, Monterey, CA; [6]NOAA/ERL/National Severe Storms Laboratory, Boulder, CO; [7]Desert Research Inst., Reno, NV; [8]NOAA/NWS/National Center for Environmental Prediction, Camp Springs, MD; [9]CIMSS/NESDIS, University of Wisconsin, Madison, WI; [10]Univ. of Oklahoma, Norman, OK

1. Introduction

Each winter numerous extratropical storms form over the Eastern Pacific ocean where limitations of the operational observing system make it difficult to monitor key meteorological conditions. Some of these storms strike the west coast of the United States (U.S.) with rainfall and winds similar to those found in land-falling tropical storms, i.e., >10 inches of rain in 24 h, and surface winds in excess of hurricane force. During stormy winter months from 1995 to 1998 in California, Oregon, and Washington such storms caused over 100 deaths, the evacuation of more than 120,000 people and at least $7 billion in damage (NOAA/National Climatic Data Center 1998). Issuance of accurate flash-flood and high-wind warnings in these events is a major forecast challenge in the region, as has been described in the summary of a recent workshop on operational requirements for a Pacific coastal forecasting system [National Weather Service (NWS) 1998]. Also, recommendations from the U.S. Weather Research Program (USWRP), and the NWS have highlighted the need for research aimed at improving such forecasts through studies related to improved quantitative precipitation forecasting (QPF), the design of an optimal observing system, and better understanding of topographic effects on local weather.

2. Experimental objectives and strategies

a) Original goals

Based on the importance of this forecast problem, and on emerging research capabilities, the California Land-falling Jets experiment (CALJET) was carried out along the California coast and up to 1000 km offshore from 1 December 1997 to 31 March 1998 (Ralph 1997). Offshore areas were observed using satellites, a NOAA P-3 research aircraft with several flight strategies (Fig. 1), drifting buoys, and 3 island-mounted wind profilers. A dense coastal observing system was deployed (Fig. 2), including two of the University of Oklahoma's Doppler on Wheels (DOW) mobile 3 cm radars, 20 boundary layer wind profilers with Radio Acoustic Sounding Systems, a vertically pointing 3 GHz (10-cm wavelength) cloud and precipitation radar, and mobile balloon soundings.

The initial objectives of the experiment were to explore the role of coastal and offshore observations of low-level jets (LLJ) and their mesoscale environment in land-falling winter storms on mesoscale quantitative precipitation and wind forecasting. As has long been recognized by operational weather forecasters in the region, the LLJ plays a key role in determining coastal rainfall, likely because orographic rainfall is strongly affected by the speed, orientation, and moisture content of the low-level flow as it encounters the coastal mountains. However, these parameters are poorly known even shortly before a storm makes land fall. At the core of the experimental design were two key objectives:

- to better understand the underlying physical processes that cause heavy rains and strong winds in this region of complex coastal topography, and
- to explore the effectiveness of possible future observing systems on 0-24 h mesoscale QPF and wind forecasts during the approach and landfall of oceanic winter storms arriving from the data-sparse eastern Pacific Ocean.

These goals were addressed using a NOAA P-3 aircraft with its in situ, radar, and GPS dropsonde data to carry out a "pre-landfall" flight strategy (Figs. 1 and 3). This strategy focused on determining precisely the location, orientation, intensity, and moisture content of the LLJ 0-24 h before its land fall, as well as the meso-α-scale environment around the LLJ that controls its evolution through deformation, confluence, and frontogenesis processes. Analysis of the damaging New Years Day storm of 1997, including the use of an MM5 simulation and the MM5 adjoint, helped confirm that the LLJ was an important player, and that it would be within reach of the aircraft 12-24 h before making landfall (Ralph et al. 1998; Bao et al. 1998). An example of this type of flight is shown in one of the major storms that produced over 10 inches of rain in 24 h (Fig. 4). Additional wind data were gathered by satellite through feature-tracking in

*Corresponding author: NOAA/ERL/Environmental Technology Laboratory, Mail code R/E/ET7, 325 Broadway, Boulder, CO 80303. tel 303-497-7099, mralph@etl.noaa.gov

GOES satellite imagery (Veldon et al. 1997). These aircraft and satellite wind data, along with drifting buoy and other satellite measurements, will be used to explore the impact of various observations on weather prediction (a.k.a. "data impact studies"), and in analyses.

Another flight strategy was carried out over the coast to complement the land-based coastal observing system. These "landfall" flights explored physical processes such as blocking, orographic rainfall, and coastal frontal occlusions, and provide data for precise model verification of kinematic, thermodynamic, and microphysical conditions. While several flights were devoted entirely to measuring conditions at landfall, some of the pre-landfall flights also made measurements along the coast while returning to Monterey at the end of their primary mission.

b) Goals related to the strong El Niño of 1997/98

Because a strong El Niño developed after the initial experimental design was complete, and such conditions are well correlated with very wet winters in California (Livezy et al. 1997), new objectives were incorporated into the experiment. These centered on assessing the role of coastal air-sea interactions on the evolution of storms and their resulting rainfall as they crossed and interacted with a 2-3 °C warm coastal sea surface temperature anomaly that could enhance the supply of low-altitude moisture and heat just upstream from the area of heavy orographic rain. This was done by adding extensive observations of the evolving "ocean mixed layer" using aircraft expendable bathythermographs (AXBTs), and by carrying out flights to measure the role of air-sea fluxes in "preconditioning" the environment for cyclogensis (Fig. 3). Fluxes were measured using turbulence data from 3-4 flight legs stacked vertically through the boundary layer and its cap.

In addition, offshore data were gathered in more approaching storms for direct use by weather forecasters and for insertion into numerical weather prediction models to aid in 0-24 h weather prediction. This objective also led to a one month extension of the special observing period, and to the development of a hybrid targeting strategy based on combining information from an ensemble-based mesoscale targeting technique with the original targeting approach that was based on underlying physical principles and mesoscale adjoint modeling. This hybrid strategy led to "extended pre-landfall" flights that reached farther offshore (Fig. 1).

3. The field phase

The strong El Niño continued through the winter, and coastal California received far above normal rainfall. This rainfall peaked during January and February 1998 while the P-3 and Doppler on Wheels were deployed (Fig. 5). In fact, it was the wettest February in California's recorded history, including Santa Barbara, which has the longest rainfall record in the state (over 130 y). Across California, three storms produced >10 inches of rain in 24 h, and extensive flooding occurred, causing 19 flood-related deaths and 33 weather-related deaths overall statewide (NOAA/NCDC at www4.ncdc.noaa.gov). From $360-550 million in damage has been reported (NOAA/NCDC or California Governor's Office of Emergency Services at www.oes.ca.gov), and statewide, 40 counties were declared Presidential Major Disaster areas.

Figure 5 summarizes the observed rainfall on each day of the experiment using two key sites, one in central California and one in northern California. There were 14 days on which more than 3 inches of rain fell in the area. Table 1 summarizes the observations during the special observing period from 18 January to 25 March 1998 in terms of the 26 P-3 flights that were flown and the supplemental coastal data that were collected.

4. Summary and future outlook

The experimental objectives led to an observing system that combined many types of measurements of the ocean and atmosphere, as well as real-time mesoscale numerical modeling, and real-time communication of the experimental data to weather forecasters and operational numerical weather prediction models. In this respect CALJET implemented an experimental system that was integrated not only in the sense of observing systems, but also in terms of its combined operational and research objectives. This was accomplished by integrating surface-based, aircraft, and satellite measurement systems. Real-time communication of data from the P-3 aircraft, wind profilers, drifting buoys, and satellite winds for operational weather forecasting was accomplished. In a case where the P-3 measured a 40 m s^{-1} LLJ on 2 February 1998, forecasters used this information to help issue an accurate flash flood warning that provided 8 h advance warning of an impending flash flood.

The data will be used to:

- explore what mix of observations, and which strategies for data assimilation, are optimal for short-term (0-24 h) weather forecasting on the U.S. west coast in winter;
- understand the role of the low-level jet in creating disruptive coastal weather;
- determine the impact of blocking on coastal winds and rain;
- improve real-time rain rate estimation by NEXRAD in complex coastal terrain; and
- measure the role of moisture and heat fluxes from the coastal ocean in producing heavy coastal rain.

Because the data were collected during a period of very heavy rains, it is possible to explore not only the QPF problem under normal conditions, but also those characterized as extreme events, i.e., those that cause some of the greatest disruption to society. It is hoped that this data set can help determine what an optimal observing system would look like for future 0-24 h mesoscale prediction of significant weather events affecting the U. S. west coast, a region that is home to 40 million people and the 8th largest economy in the world.

References

Bao, J.-W., J. M. Wilczak, and F. M. Ralph, 1998: Sensitivity of coastal prediction to uncertainties in the strength and location of the low-level jet. *12th Conf. on Numerical Weather Prediction*, Phoenix, AZ, Amer. Meteor. Soc., 69-72.

Livezey, R. E., M. Masutani, A. Leetmaa, H. Rui, M. Ji, and A. Kumar, 1997: Teleconnective response of the Pacific-North American region atmosphere to large central equatorial Pacific SST anomalies. *J. Climate*, **10**, 1787-1820.

National Weather Service, 1998: Workshop on Pacific Coastal Forecasting System Operational Requirements. Ed. P. Hirschberg. 19-21 August 1997, Monterey, CA. [Available from US Dept. of Commerce, NOAA/National Weather Service, Office of Meteorology, Silver Spring, MD.]

NOAA/National Climatic Data Center, 1998: Billion dollar U.S. weather disasters 1980-1998. www.ncdc.noaa.gov/ol/reports/billionz.html.

Ralph, F. M., 1997: The California Land-Falling Jets Experiment CALJET. Goals and Experimental Design.[http://www7.etl.noaa.gov/programs/CALJET/index.html or NOAA/ETL, 325 Broadway, Boulder, CO 80303; e-mail: mralph@etl.noaa.gov]

Ralph, F. M., P. J. Neiman, P. O. G. Persson, and J.-W. Bao, 1998: Observations of California's New Years Day storm of 1997. *2nd Conf. on Atmos. and Ocean. Prediction and Processes*, 11-16 Jan., Phoenix, AZ, AMS, 219-224.

Veldon, C. S., C. M. Hayden, S. Neiman, W. P. Wenzel, S. Wanzong, and J. S. Goerss, 1997: Upper-tropospheric winds derived from geostationary satellite water vapor observations. *Bull. Amer. Meteor. Soc.*, **78**, 173-195.

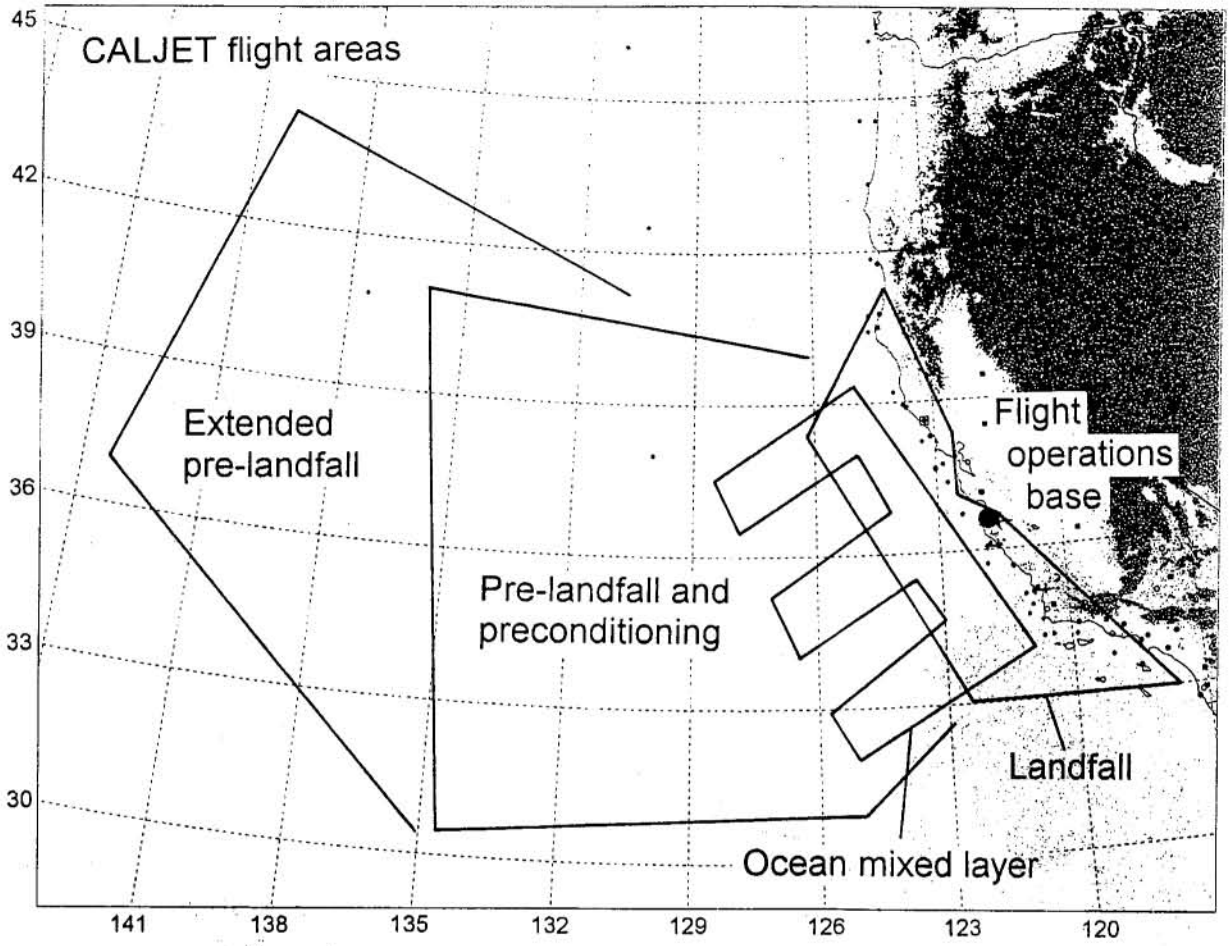

Fig. 1. Outline of flight areas based on flight objectives. Each domain is marked based on the farthest extent of all flight tracks with a common primary flight objective.

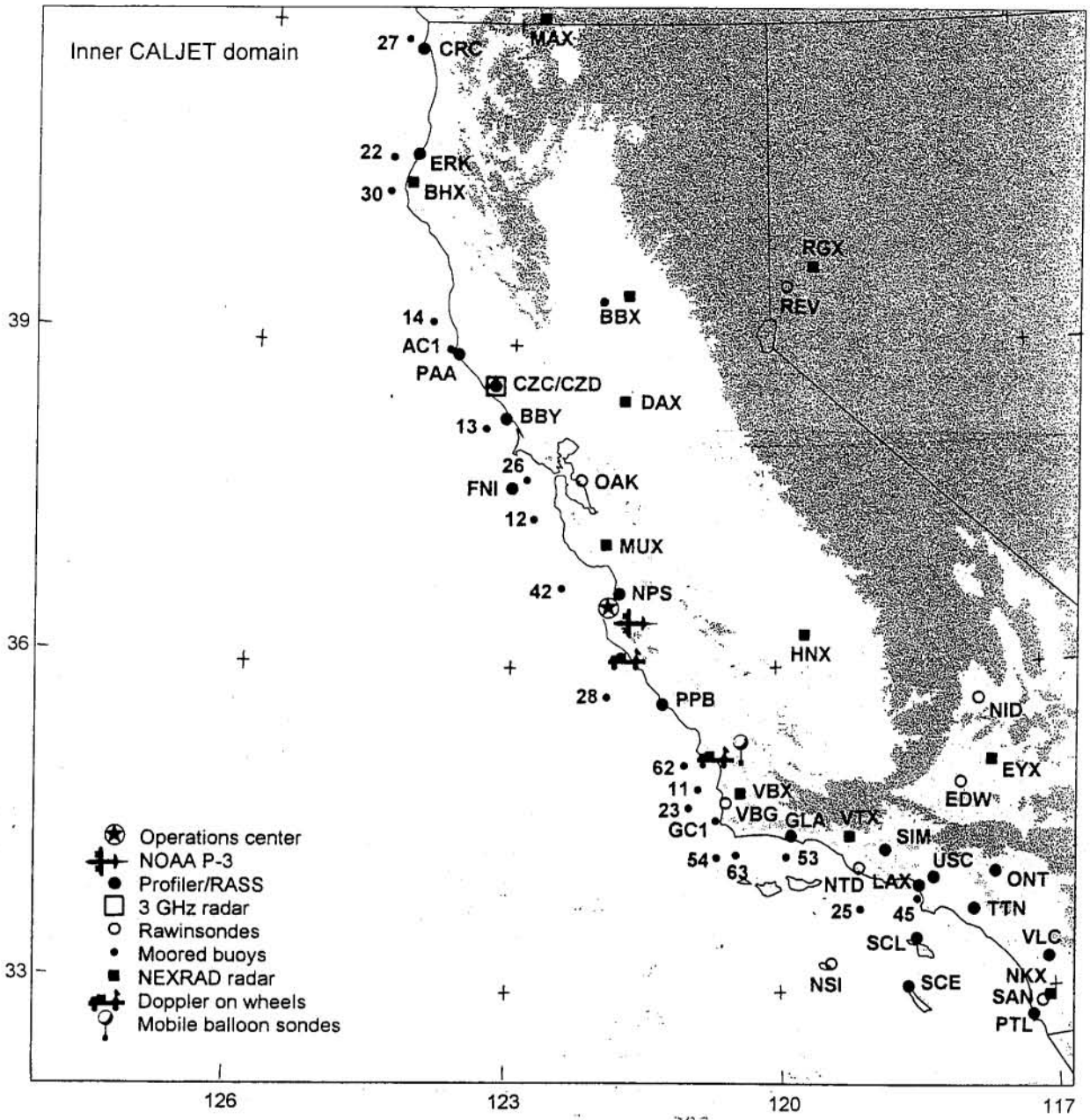

Fig. 2. Base map showing the coastal observing system during CALJET, including experimental and key operational observing sites.

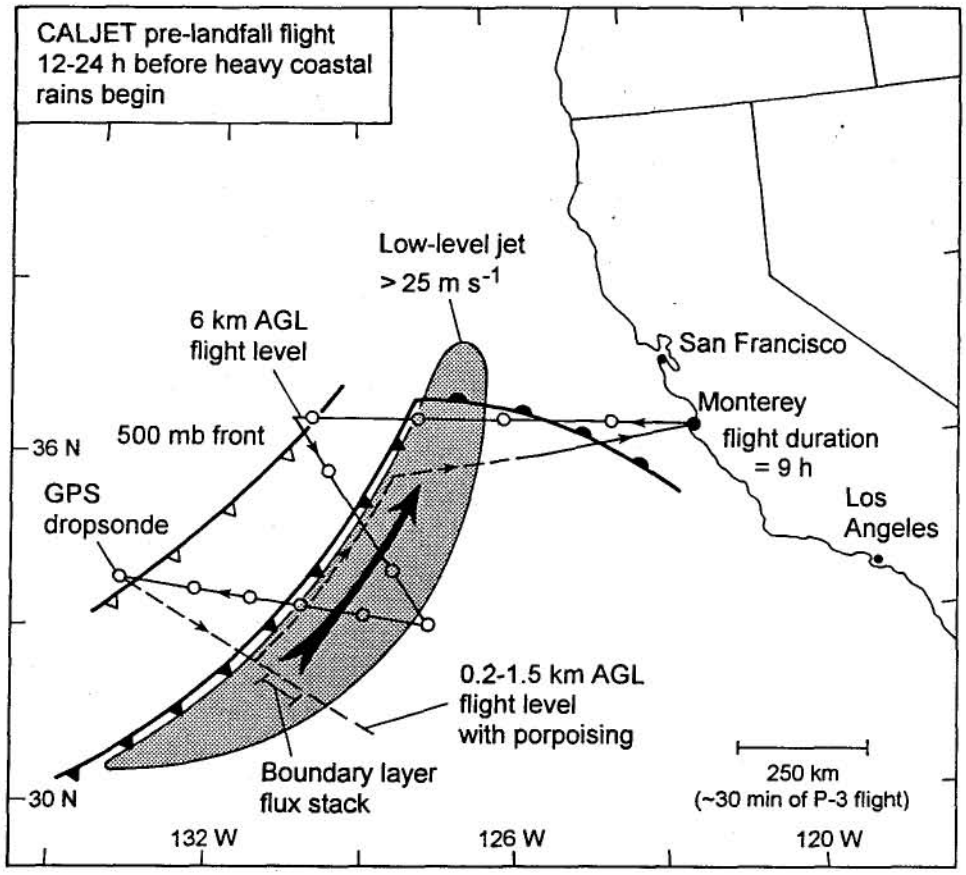

Fig. 3. Schematic illustration of the pre-landfall flight strategy designed to measure the location, intensity, moisture content and mesoscale environment surrounding the pre-cold frontal low-level jet while a storm was still well offshore. Missions started with mid-tropospheric (~6 km or 500 mb) flight legs and GPS dropsondes, followed by a descent to ~500 m altitude on the cold side of the surface front. After penetrating the surface cold front, the LLJ was mapped out in the vertical, cross-front and along-front dimensions. Surface fluxes were measured in the warm sector using stacked flight legs.

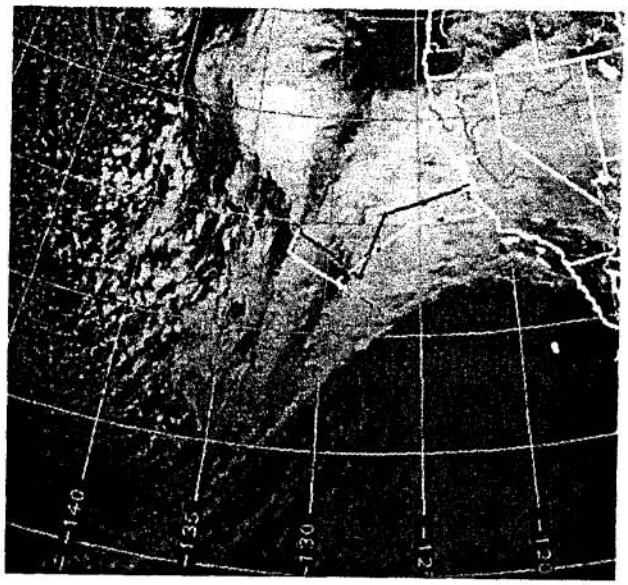

Fig. 4. Infrared satellite image at 1830 UTC 2 February 1998 with the flight track of the NOAA P-3 superimposed. Dark (white) areas of the track are legs above (below) 1.5 km altitude. Dots along dark flight leg mark dropsonde locations. The image corresponds to the end time of the flight, which had begun at 1025 UTC. This storm produced >300 mm (12 inches) of rain just south of Monterey in the 24 h following the end of the flight.

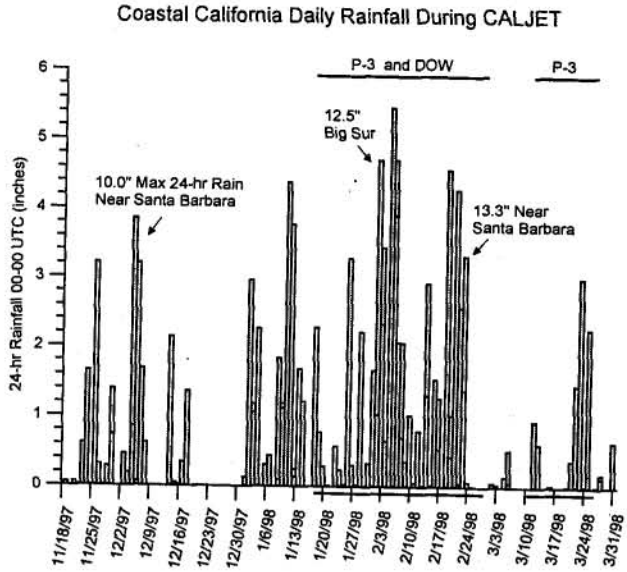

Fig. 5. Precipitation during the experiment is summarized using 24-h accumulated rainfall at Cazadero (CZD), and at Goleta (GLA). For each day, the greatest value is shown. Site locations are in Fig. 2. Times at which the NOAA P-3 aircraft and the two University of Oklahoma DOW were in California are marked at the top and bottom of the figure. Dates (mm/dd/yy) are shown along the abscissa. The three heaviest rain events are marked.

Table 1. Overview of Intensive Observing Periods (IOPs) during CALJET, as defined by P-3 research flights.

IOP	Type of flight	Take off date (mm/dd)	Take off time (UTC)	Landing date (mm/dd)	Landing time (UTC)	Drop-sondes (#)	AXBTs (#)	Flux stacks (#/#⁺)	Extra soundings (site/#⁰)		Doppler on Wheels (S=single D=dual)	GOES winds
1	L	01/18	1830	01/19	0200	2	10	3/0	M5		0	A
2	L	01/19	1753	01/19	2347	1	4	2/0			0	A
3	O	01/20	1809	01/21	0332	0	65/57*	0/10			0	B
4	P	01/23	1358	01/23	2303	10	2	1/1	M3		Eureka (S)	A
5	PN	01/25	2002	01/26	0445	30	0	0/0			(S)	B
6	L	01/26	2051	01/27	0255	0	0	0/0	M9		Bodega Bay (D)	A
7	L	01/28	2044	01/29	0400	0	4	3/3	M1		0	A
8	P	02/02	1025	02/02	1835	10	2	1/3	M4	P6	Big Sur/south (D)	A+SRS
9	PL	02/03	1139	02/03	1929	5	2	1/0	M6	P4	Big Sur/Goleta (D)	A
10	P	02/05	1912	02/06	0405	13	4	1/1			0	A+SRS
11	F	02/06	1902	02/07	0331	4	6	4/0			Bodega Bay (S)	A+SRS
12	P	02/09	2243	02/10	0743	12	4	2/0	M5		0	A
13	O	02/11	1612	02/12	0112	0	86/47*				0	A
14	L	02/12	1933	02/13	0108	2	0	0/2	M5		Big Sur (D)	A
15	P	02/13	2322	02/14	0907	12	3	1/0			(S)	B
16	PL	02/16	2021	02/17	0510	8	3	3/1	M5		Big Sur/Goleta (D)	A
17	PL	02/19	1246	02/19	2122	11	2	2/0	M3		Bodega Bay (S)	B
18	F	02/22	1456	02/22	2353	2	2	5/0	M6		0	B
19	L	02/23	1603	02/23	2101	2	0	0/1		P9	Goleta (S)	A
20	O	02/26	1653	02/27	0215	0	85/47*					A
21	PE	03/11	1953	03/12	0509	14	0	1/0				C
22	PL	03/12	2258	03/13	0420	5	0	0/0				B
23	PE	03/21	1900	03/22	0445	13	19	0/1				C
24	PE	03/22	2058	03/23	0628	15	15	0/0				C
25	PE	03/23	2200	03/24	0710	23	0	0/0				A
26	PE	03/24	2300	03/25	0820	19	27	0/0				A
Total		P-3: 217 h research +18 h ferry				213**	345	30/27⁺	52	19	150 h total^	

L: pure land fall (6)
O: ocean mixed layer survey (3)
P: pure pre-land fall (5)
PN: pre-land fall with NORPEX (1)
PL: combined pre-land fall and land fall (4)
F: preconditioning fluxes (2); PE: extended pre-land fall (5)

*number that were successful
**17 failed
⁰M:mobile; P:Point Mugu & San Nicholas Is.
^40 h of possible dual Doppler data
⁺full stacks/partial stacks

GOES data availability
A: excellent
B: good
C: limited
SRS: super rapid scan

8.2 OBSERVATIONS OF THE STRUCTURE OF THE LOW-LEVEL JET IN LANDFALLING WINTER STORMS USING THE CALJET OBSERVATIONAL NETWORK

O. Persson[1], M. Ralph[2], B. Walter[3], P. Neiman[2], C. King[2], A. White[1], and J. Wilczak[2]

[1]Cooperative Institute for Research in Environmental Sciences/NOAA/ETL, Boulder, CO
[2]NOAA/Environmental Technology Laboratory, Boulder, CO
[3]NorthWest Research Associates, Bellevue, WA

1. INTRODUCTION

A primary objective of the California Land-Falling Jets Experiment (CALJET) was to study the structure of the low-level jet (LLJ) within landfalling storms and relate this structure to heavy coastal precipitation. CALJET was conducted along the California coast and over the eastern North Pacific Ocean during the winter of 1997-98. Because this winter was influenced by a strong El Nino event numerous storms occurred and extensive measurements were obtained from the coast up to 1000 km offshore. Offshore observations of the evolving LLJs were made using measurements from satellites and the NOAA P-3 research aircraft, and nearshore observations were provided by these platforms as well as the extensive land-based ones, which feature a coastal array of 915 MHz wind profilers. The large integrated observing system is described by Ralph et al (1999).

Using several of CALJET's observational platforms, this presentation describes the LLJ structure of a storm measured offshore on February 2, 1998, and then again at landfall on February 3.

2. OFFSHORE STRUCTURE

Offshore, the developing storm system consisted of a baroclinic zone with a very complex structure. Two main southwest-to-northeast oriented cloud bands were evident, labeled I and II in Fig. 1, as well as a "cloud-head" further to the northwest. Cloud-tracked winds (Veldon, *et al* 1997) at heights above 1 km show a horizontal wind shear across Bands I and II, suggesting that these bands marked the baroclinic zone. The developing low-pressure area was probably located near where Band II intersected the cloud-head, with a developing warm front and the associated overrunning extending eastward towards the California coast. For the first 3 hours of its flight, the NOAA P-3 aircraft deployed dropsondes from about 5.5 km altitude within the warm-frontal region and near the northeastern ends of the two main cloud bands. At about 1330 UTC, the aircraft descended to low levels, and remained below 1500 m for the rest of the flight.

The complex offshore structure of the LLJ region in this developing system is revealed by the aircraft pass at 430 m from Band II towards the southeast at 1400-1515 UTC, and the subsequent stacked legs and aircraft "soundings" in Band I between 1515-1615 UTC. Along the 500 km distance of the pass, the wind and thermodynamic data show that the low-level air in Band II is 4-5 K cooler than in Band I, the wind speed is much weaker (Fig. 1), and the wind direction is from the southeast rather than from the south-southwest. Surprisingly, in the gap between the bands, a moderately strong (18 m s^{-1}) northerly wind was observed. Hence, the system appears to consist of strong small-scale features and is not well organized yet on the larger scale.

The transition from the cooler/ lower momentum air to the northwest to the warmer/higher momentum air to the southeast occurs at two points about 40 km apart on the northwest side of Band I (Fig. 2). The first point, called the thermodynamic front (TF), is where the temperature and humidity increase substantially. It is associated with a brief period of upward motion of 1 m s^{-1}. Also, the wind direction shifts to southerly or south-southwest and increases to about 16 m s^{-1}. The very strong winds, however, are not found until about 40 km farther to the southeast. The kinematic front (KF), marked by a vertical velocity of about 3 m s^{-1}, is the northwest edge of a 200 km wide region of 30 m s^{-1} low-level winds and enhanced turbulence (Fig. 2b). This region is the LLJ, and is marked in the satellite images by most of Band I. It is unusual for the thermodynamic front and the kinematic front to be separated by this much. A separation of about 5 km is more common (e.g., Hobbs and Persson 1982).

An extensive cross-sectional flight pattern was performed in the LLJ, including a stack of 4 legs each about 60 km long just to the SE of the kinematic front in the strongest winds (Fig. 2a). An AXBT provided a reliable measurement of the sea surface temperature (SST), which would have been difficult to obtain with the downward-pointing radiometer because of the rain, clouds and sea-spray. The flight pattern showed that the axis of the LLJ was at about 970 m with the strongest wind of 36 m s^{-1} located nearest the KF. Using the averages across the 4 stacked legs and the SST measurement, vertical profiles of various thermodynamic and turbulent quantities were obtained, revealing the vertical structure of the LLJ (Fig. 3). The cloud base varied between 450-720 m, with the lower base nearest the KF. The atmosphere was weakly stable to dry lifting ($\partial\theta/\partial z > 0$), but had significant potential instability (PI; $\partial\theta_e/\partial z < 0$). Hence, any saturated plumes would be buoyantly unstable in the lowest 1000 m below the LLJ axis. Through most of the boundary layer below cloud base, the dry stability was also weak enough

Corresponding author: Dr. Ola Persson, CIRES/NOAA/ETL, 325 Broadway, Boulder, CO 80303. E-mail: opersson@etl.noaa.gov

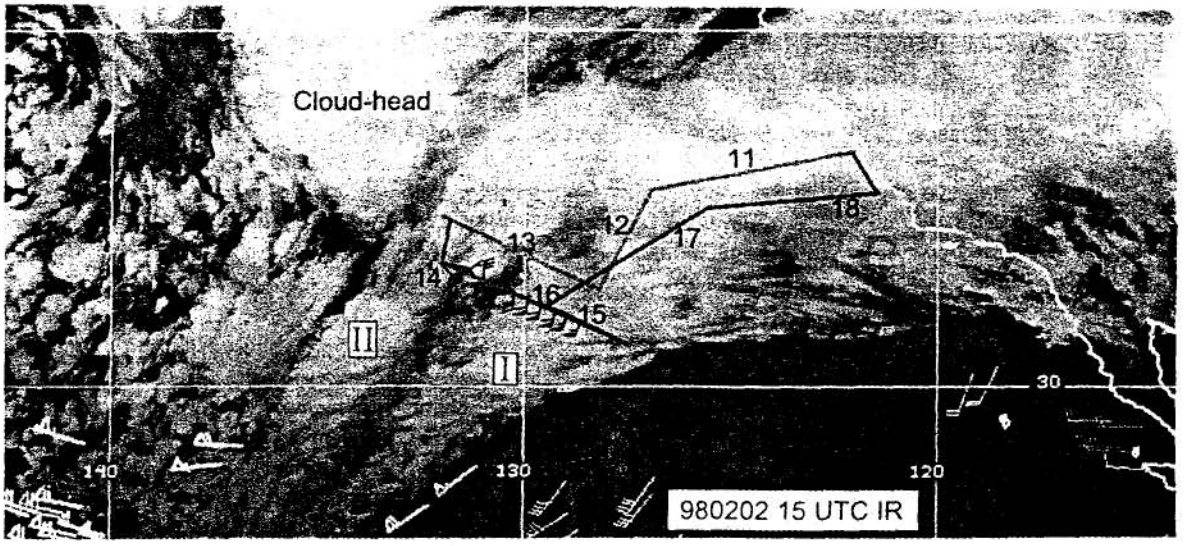

Fig. 1: GOES-9 infrared image at 15 UTC Feb. 2 showing cloud Bands I and II, cloud-track winds (large wind barbs), the P-3 flight track with hours marked, and flight level winds along the 430 m leg between 14-15 UTC.

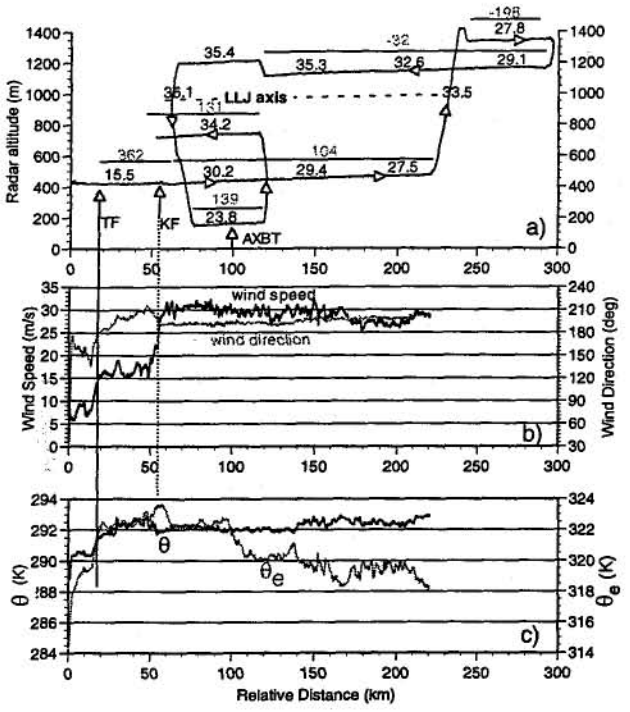

Fig. 2: Flight track and flight-level data in Band I. Shown are a) flight track (time-space adjusted), mean wind speeds (dark numbers; m s^{-1}) for about 10-min segments and latent heat fluxes (light numbers; W m^{-2}), b) wind speed and wind direction, and c) potential (θ) and equivalent potential(θ_e) temperatures (K) along the 430 m flight leg.

and the vertical shear strong enough that the Richardson number was below the critical value of 0.25, indicating that mechanical mixing was most likely also occurring. Enhanced turbulence was observed on the lower legs. Though generally corroborating this vertical structure, three individual ascent/descent profiles in the LLJ at different distances from the KF (see Fig. 2a) show that the PI is strongest along the southeastern side of the LLJ because the air is drier there than near the KF.

Direct turbulent latent heat flux measurements show moderately large upward latent heat fluxes of 130-140 W m^{-2} in the LLJ nearest the KF, but 2-3 times this value near the thermodynamic and kinematic fronts (Fig. 2a). Hence, significant moisture is being added to the LLJ region. Turbulent sensible heat fluxes were not measured, but bulk estimates based on Fig. 3 suggest that they should be about 5-10 W m^{-2} directed downward, indicating a slight loss of sensible heat through turbulent processes.

The strongest observed winds in this LLJ was 42 m s^{-1} to the northeast of this cross-section at about 1630 UTC (see Figs. 1 and 5). This may either indicate along-front variability or a strengthening of the LLJ.

3. LLJ STRUCTURE NEAR LANDFALL

During the next 24 hours, the storm developed and moved eastward. Band II dissipated and was no longer discernible after 03 UTC, 3 Feb. Band I, however, remained distinct, rotated to be oriented nearly meridional, and moved east-northeast. It came onshore in central

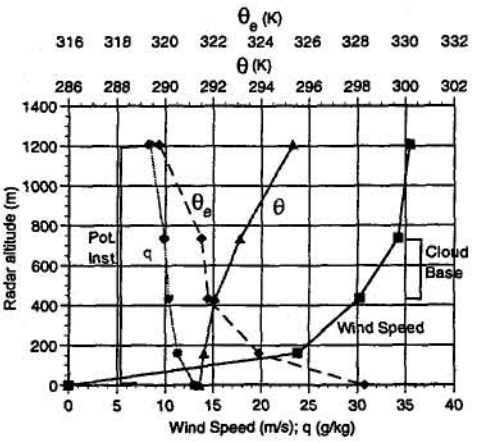

Fig. 3: Vertical profiles constructed from mean values along the flux stack legs just SE of the kinematic front in 2a.

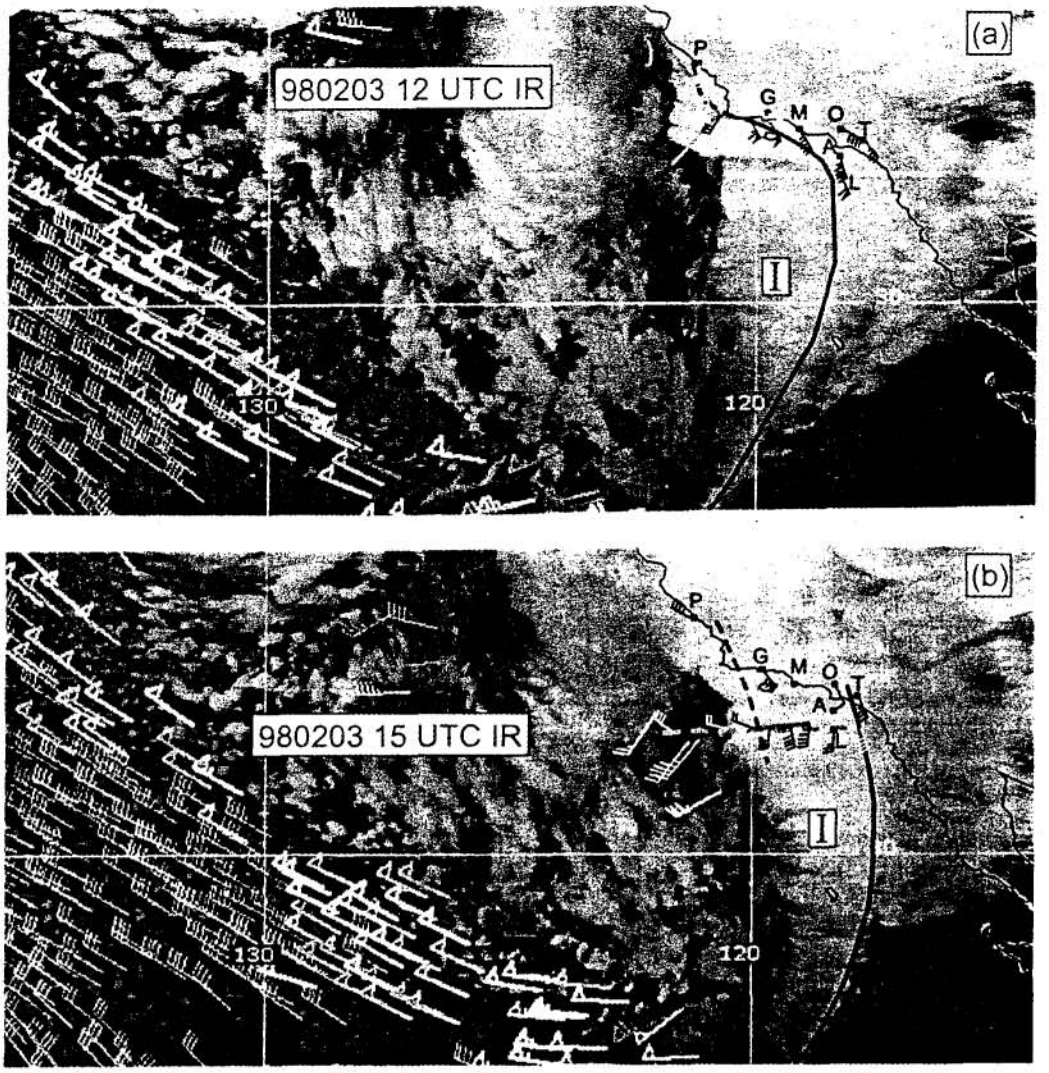

Fig. 4: GOES-9 infrared image at a) 12 UTC and b) 15 UTC Feb. 3. The main windshift line is solid, and the secondary line is dashed in b). Small wind barbs show the wind at about 450 m MSL, except for the white barbs in a) which are at other levels and are discussed in the text. Only data within a 3-hour window centered on the above times are used. The wind profiler and surface data sites are Pt. Piedras Blancas (P), Goleta (G), Los Angeles (O), Tustin (T), Santa Catalina Island (A) and San Clemente Island (L). A sounding was done at Pt. Mugu (M). Large wind barbs show the cloud-track winds. In b), the light dashed line shows the flight track during the dropsonde cross-section, the light solid line shows the location of the P-3 stacked legs, and the small white barbs show dropsonde winds.

California near 06 UTC and then later affected southern California between 09-21 UTC (Fig. 4). Heavy rainfall occurred in central and southern California in conjunction with this cloud band, including 300 mm in the 24 hours ending at 19 UTC 3 Feb. in the mountains along the Big Sur coast.

The next P-3 flight was done in the California Bight region between 1130-1930 UTC, 3 Feb. This flight included two legs at 650 m and 1580 m in the Santa Barbara Channel near Goleta at 1233-1305 UTC (Fig. 4a), a dropsonde cross-section at 1335-1420 UTC and a flux stack consisting of 5 legs at 1432-1602 UTC further upwind of the Santa Barbara coastline (Fig. 4b). These legs were all through Band I. The position of the dropsonde cross-section has been time-space adjusted eastward. In addition, wind profiler and surface meteorology data were obtained at six sites (see Fig. 4), while special soundings were launched at Goleta and Pt. Mugu. Surface data are shown at profiler sites where velocity folding in the profiler data has not yet been corrected.

South of the Channel Islands, the strongest low-level winds occur ahead of Band I rather than within it, in contrast to the structure offshore. At San Clemente Island, 29 m s^{-1} winds from the SSE were seen at 450 m for a few hours prior to 13 UTC (Fig. 4a). This strong wind is associated with a LLJ reaching 31 m s^{-1} at 700-1100 m altitude (Fig. 5). The westward curvature of the windshift line and the LLJ region within the Santa Barbara Channel towards the west side of Band I is supported by the presence of a strong LLJ in the 1147 UTC sounding at Pt. Mugu and the SE winds of 27-35 m s^{-1} observed by the P-3 at 650 m MSL over the Santa Barbara Channel. At Goleta, the surface (10 m) wind was 18 m s^{-1} from the

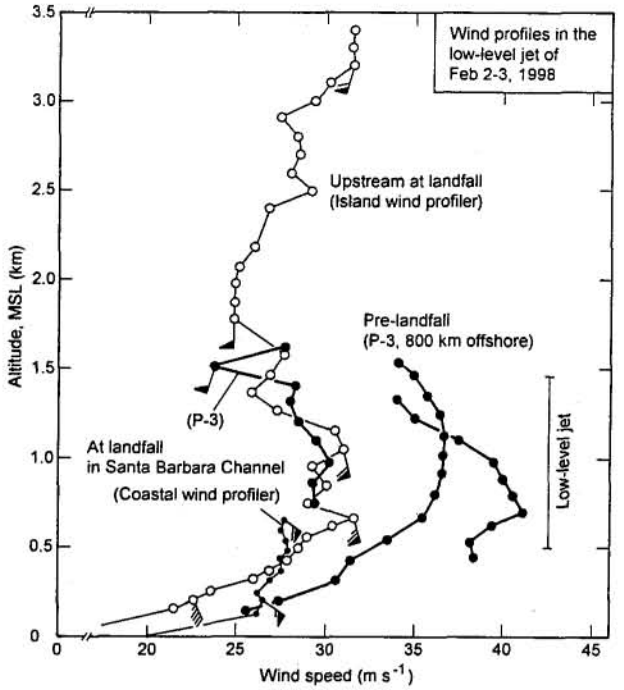

Fig. 5: Wind profiles in the LLJ regions both offshore (Pre-landfall, 1619-1628 UTC 2 Feb.) and nearshore (at landfall). The "island wind profiler" is San Clemente Island. The "coastal wind profiler" is Goleta. Profiler data are 1-h averages from 11-12 UTC 3 Feb. Selected wind barbs are shown.

ESE. The continuation of this windshift line north from Pt. Conception is suggested by the 15 m s^{-1} SSE surface wind at Pt. Piedras Blancas and the small area of 30-35 m s^{-1} SSE winds measured by the P-3 NNW of Pt. Conception at 1600 m (Fig. 4a). A similar wind shift was noted by the P-3 at the same height in the Santa Barbara Channel. Hence, it appears as if the LLJ region at 12 UTC is located east of Band I south of the Channel Islands, and is pinched between the west edge of Band I and the coastline north of Pt. Conception and south of Pt. Piedras Blancas. The transition from the east side to the west side appears to occur near the Santa Barbara Channel, where the LLJ region is pinched against the steep coastline. This interpretation is still uncertain and will be further evaluated using the airborne radar, the mobile land-based radars, surface data from other coastal sites, additional thermodynamic soundings available at Goleta, and the unfolded profiler data.

Within Band I, the winds are generally 13-20 m s^{-1} from the south (Fig. 4b), which is consistent with a decrease in wind speed and a veering of the wind at Goleta, Santa Catalina Island, and San Clemente Island between 1230 and 1330 UTC. At the two latter sites, precipitation only occurred as Band I moved over the sites after the windshift. Further to the west along the western edge of Band I, another windshift marks the transition to weaker westerly or northwesterly winds. The southwesterly cloud-track winds near the western end of the flight track are at 600-850 mb.

Though the winds within Band I south of the Santa Barbara Channel are weaker than those ahead of it, the

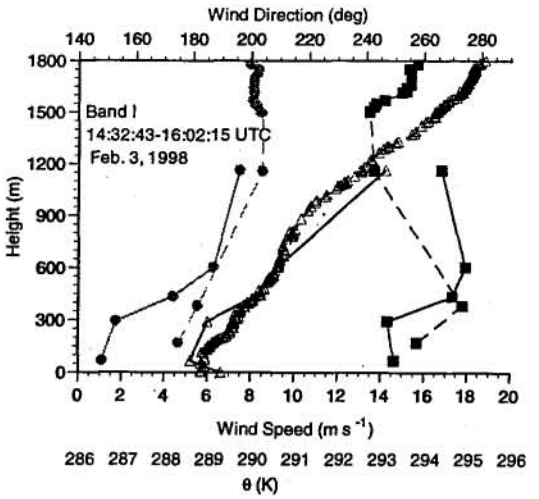

Fig. 6: Profiles of wind speed (squares), wind direction (dots) and potential temperature (θ; triangles) using mean values from the five flux stack legs (solid) and the dropsondes (dashed) within the southerly flow in Band I.

region within Band I still appears to have the characteristics of a LLJ region (Fig. 6). A wind maximum of about 18 m s^{-1} occurs at 700-1000 m altitude, the wind direction veers with height indicating warm advection, and the lower atmosphere is slightly stable suggesting the northward advection of warm air over slightly cooler water. These are all characteristics of the LLJ region in Band I observed offshore on the previous day.

3. WORK IN PROGRESS AND FUTURE PLANS

Further analysis of the nearshore data from the flux stack, the dropsonde cross-section, wind profilers, etc., is in progress and will be used to examine the two LLJ regions present in the landfall of this storm system. In addition, validation of the structure suggested in the analysis above will be made. Finally, more detailed examination of the small-scale structure of the transition zone within the California Bight is planned for this case and for several other landfalling storms which exhibited similar evolutions. These analyses should lead to a better understanding of the influence of the complex topography on the structure and precipitation distribution of land-falling storms in heavily populated southern California.

4. REFERENCES

Hobbs, P. V. and P. Ola G. Persson, 1982: The mesoscale and microscale structure and organization of clouds and precipitation in midlatitude cyclones. Part V: The substructure of narrow cold-frontal rainbands. *J. Atmos. Sci.*, **39**, 280-295.

Ralph, F. M., P. O.G. Persson, D. Reynolds, W. Nuss, D. Miller, J. Schmidt, D. Jorgensen, J. Wilczak, P. Neiman, J.-W. Bao, D. Kingsmill, Z. Toth, C. Veldon, A. White, C. King,, and J. Wurman, 1999: The California Land-falling Jets Experiment (CALJET): Objectives and design of a coastal atmosphere-ocean observing system deployed during a strong El Nino. *Preprints, 3rd Symp. on Integrated Observing Systems.*, Jan. 10-15, 1999, Dallas, TX.

Veldon, C. S., C. M. Hayden, S. Neiman, W. P. Wenzel, S. Wanzong, and J. S. Goerss, 1997: Upper-tropospheric winds derived from geostationary satellite water vapor observations. *Bull. Amer. Meteor. Soc.* **78**, 173-195.

8.5

PRECIPITATION MICROPHYSICS OBSERVED DURING THE 5-6 FEBRUARY STORM OF CALJET

A. White [1*], P. Neiman [2], C. King [2], J. Jordan [2], M. Ralph [2], O. Persson [1]

[1] Cooperative Institute for Research in Environmental Sciences
University of Colorado/NOAA Environmental Technology Laboratory, Boulder, CO

[2] NOAA Environmental Technology Laboratory, Boulder, CO

1. INTRODUCTION

During the winter of 1997-98, scientists from the NOAA Environmental Technology Laboratory (ETL) deployed 13 integrated observing systems, including one near Cazadero, CA (CZD) and one near Bodega Bay, CA (BBY) (Fig. 1) in support of the California Land Falling Jets Experiment (CALJET) (Ralph et al., 1999). In this paper we demonstrate the synergistic nature of the data collected with these tools by presenting an analysis of measurements taken during the storm that occurred on 5-6 February 1998. The analysis focuses on ways in which the precipitation intensity and microphysics responded to mesoscale forcing. These detailed measurements are also part of an effort to improve real-time quantitative precipitation estimation (QPE) by NEXRAD radars in this flood-prone region.

2. OBSERVING SYSTEMS

The observing system deployed at CZD consisted of a 915-MHz wind profiler with a Radio Acoustic Sounding System (RASS), a vertically-pointing S-band (3 GHz) radar, a laser ceilometer, and a suite of surface meteorological instruments comprising pressure, temperature, relative humidity, wind speed and direction, and radiation (solar and net) sensors mounted on a 10-m tower along with a tipping-bucket rain gauge. The observing system at BBY incorporated the same instruments as at CZD, minus the 3-GHz radar. The wind profiler, ceilometer, and tower instruments were all commercially available and represented the industry standard at the time of CALJET.

The ETL S-band radar was developed in conjunction with NOAA Aeronomy Laboratory engineers (Ecklund et al., 1995). This frequency band is typically used to monitor precipitation echoes, but it also has been used to observe the more strongly reflecting regions of clouds (e.g., Knight and Miller, 1993). The ETL system uses a single linear receiver, which we anticipated would saturate during the heavier precipitation events encountered during CALJET. To address this problem, ETL engineers included a coupler at the input to the receiver that reduced the incoming signal by 30 dB.

In order to maximize the information received from the S-band radar and, thereby, increase its benefit to CALJET, we programmed the radar to alternate between three operating modes: a light-precipitation mode with no pulse coding and without the coupler, a heavy-precipitation mode with no pulse coding and with the coupler, and a high-sensitivity mode with an 8-bit pulse code, resulting in a 6-dB enhancement in average power. The measurements presented in this paper are from the heavy-precipitation mode, which profiled to a height of 4.3 km above ground level (AGL) using 40 range gates with 105-m vertical resolution. The Nyquist interval, or folding velocity, was ±12.5 m s^{-1}. White et al. (1998) provided a calibration for the ETL S-band radar and estimated the radar sensitivity in the high-sensitivity mode to be -14 dBZ at 10 km, or -34 dBZ at 1 km.

3. THE FEBRUARY 5-6 STORM

3.1 Synoptic and Mesoscale Overview

The cyclone studied here was one in a series of powerful storms intensively observed during CALJET that battered the California coast during the winter of 1997-98. On 5 February, satellite imagery of the cyclone at 2000 UTC (Fig. 2) exhibited a warm-frontal baroclinic "leaf" cloud band (Weldon, 1979) extending northeastward from the subtropical Pacific Ocean to California and the CZD site. Widespread precipitation was falling beneath this cloud leaf over northern California at this time. The storm deepened rapidly to ~960 mb immediately offshore of the northern California coast on 6 February and produced strong (>30 m s^{-1}) winds in the region.

Observations from the CZD and BBY sites provided valuable mesoscale information during this 2-day event. The wind profiler and RASS measurements from CZD (Fig. 3) revealed a strong warm front from the surface to 1.3 km above mean sea level (MSL) between 1800 and 2200 UTC 5 February during the time when the warm-frontal cloud leaf was centered over the site. Prior to this time, the melting level rose from 1.7 to 2.4 km MSL, consistent with a sloping warm-frontal zone. After ~2000 UTC the melting level began descending, suggestive of a cold frontal passage aloft. With the warm front still

* *Corresponding author address*: Allen B. White, NOAA/ERL/ETL, R/E/ET7, 325 Broadway, Boulder, CO 80303; e-mail: abw@etl.noaa.gov

present below, this indicated the presence of a warm occlusion and the onset of static destabilization, which may have helped produce the second largest rainfall rate during this event. The largest rainfall rate occurred at ~1300 UTC 6 February just prior to another cold frontal passage aloft.

Both periods of heavy rain also corresponded with a 5-10 m s^{-1} onshore wind component measured in the lowest 750 m MSL on the coast at BBY. The ratio of rainfall measured at CZD (~500 m MSL) and on the coast at BBY varied from ~1:1 between 1330 and 1850 UTC 5 February when the flow was donwnslope, to ~10:1 between 2130 UTC 5 February and 0200 UTC 6 February and between 1200 and 1500 UTC 6 February when the flow was strongly upslope. This pattern suggests that large-scale upward motion resulted in nearly equal rainfall at both sites in spite of downslope conditions, but when upslope flow occurred in a region of large-scale upward motion, there was significant rainfall enhancement at the mountain site.

3.2 *S-band Radar Analysis*

Figure 4 displays time-height sections of vertical velocity (hydrometeor fall velocity) and radar reflectivity factor recorded by the S-band radar during the period 0000 UTC 5 Feb - 1600 UTC 6 Feb. The melting layer is clearly identified by the gradient in velocity and the "bright band" in radar reflectivity, and its behavior mirrors that of the melting layer observed by the collocated wind profiler.

Figure 5 shows the accumulated rainfall recorded by the rain gauge at CZD for the 40-h case-study period. To help interpret the precipitation measurements, we used time series of fall velocity and radar reflectivity factor from the S-band radar at the second range gate (centered at 263 m AGL) to classify periods of nearly constant rainfall rate. Our subjective analysis produced the 12 periods denoted by the Roman numerals in Fig. 5. We then compared the average rainfall rate during each of the 12 periods to the average radar reflectivity factor measured by the radar at 263 m AGL (Fig. 6). For comparison we included the Marshall-Palmer relation (MPR), given by $Z = 200R^{1.6}$, with rainfall R in mm hr^{-1} and reflectivity Z in $mm^6\ m^{-3}$ (Marshall et al., 1955). For $R < 10$ mm hr^{-1}, the agreement was fair with the MPR. For $R > 10$ mm hr^{-1}, the MPR substantially underestimated the rainfall rate, suggesting that the higher rainfall rates during this particular storm resulted from drop-size distributions that were weighted more heavily to the smaller drops. The two periods when the rainfall deviated most from the MPR were during periods V and X. As described earlier, these periods experienced strong lower-troposhperic warm advection and upslope flow during the approach of a cold front and associated frontal forcing aloft. Future work will determine whether these attributes contributed to the poor performance of the MPR.

4. SUMMARY

We presented an analysis of measurements obtained from two integrated observing systems deployed on the central California coast during CALJET. Figure 3 demonstrates the ability of these systems to provide important details of both the synoptic and mesoscale structure of extratropical cyclones as well as to monitor orographic rainfall enhancement and its causes. The comparison of S-band radar reflectivity measurements with rain-gauge data for one storm suggests that strong upslope flow enhances orographic rainfall by increasing the number of small drops at low altitudes (e.g., Cotton and Anthes, 1989). These altitudes are not observed by NEXRAD radars in this and other coastal mountainous regions of California because of terrain occultation. The measurements presented here will be used to help improve the QPE by NEXRAD radars in one of these important flood-prone regions.

5. REFERENCES

Cotton, W.R., and R.A. Anthes, 1989: *Storm and cloud Dynamics.* Academic Press, 880 pp.

Ecklund, W.L., et al., 1995: An S-band profiler for tropical precipitating cloud studies. *Preprints, 27th Conf. On Radar Meteor.*, Vail, CO, Amer. Meteor. Soc, 335-336.

Knight, C.A., and L.J. Miller, 1993: First radar echoes from cumulus clouds. *Bull. Amer. Meteor. Soc.*, **74**, 179-188.

Marshall, J.S., W. Hitschfeld, and K.L.S. Gunn, 1955: Advances in radar weather. *Adv. Geophys.*, **2**, 1-56.

Ralph, F.M., et al., 1999: The California Land-falling Jets Experiment (CALJET): Objectives and design of a coastal atmosphere-ocean observing system deployed during a strong El Nino. This volume.

Weldon, R., 1979: Cloud patterns and the upper air wind field. Satellite Training Services Course Notes, Part IV, Air Weather Service Document AWS/TR-79/003, 89 pp.

White, et al., 1998: S-band radar intercomparisons with Ka-band radar. *Preprints, Fourth International Symposium on Lower Tropospheric Profling,* Snowmass, CO, 326-328.

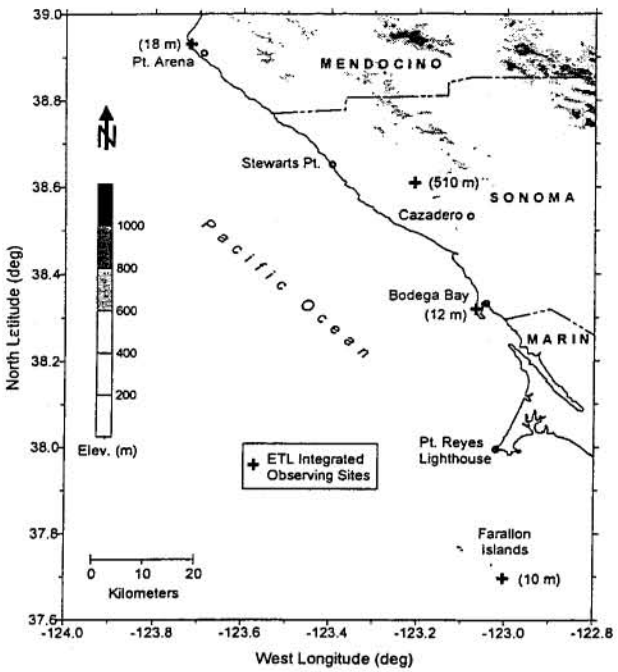

Figure 1. Map showing a portion of the CALJET domain along the northern California coastline. The locations of the integrated observing sites are denoted by plus symbols. Site elevations are listed in parentheses.

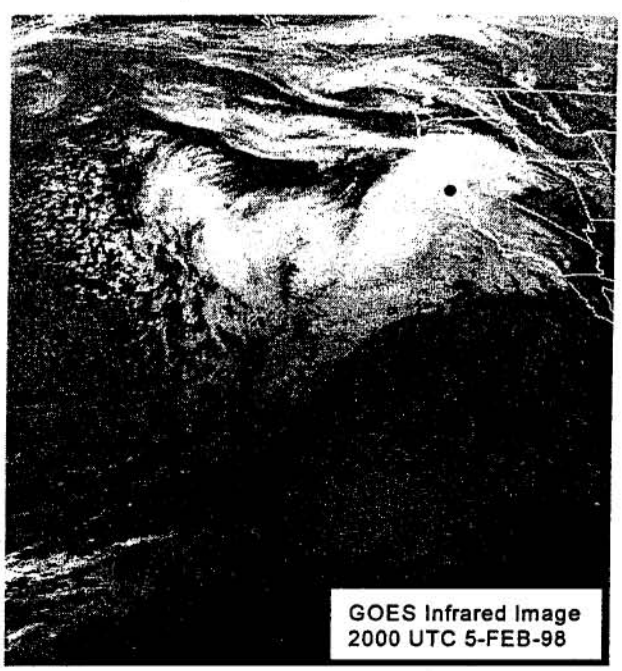

Figure 2. GOES infrared satellite image at 2000 UTC 5 February 1998. The bold dot marks the integrated observing site at CZD.

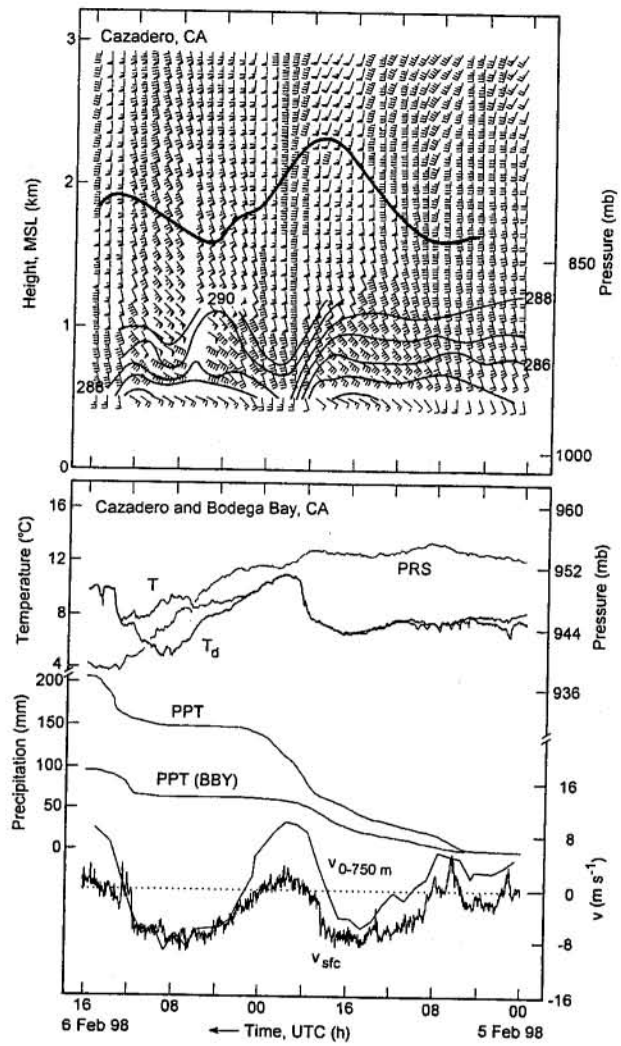

Figure 3. Upper panel: time-height section of hourly RASS virtual potential temperature (K); hourly consensus horizontal winds (flags = 25 m s^{-1}, barbs = 5 m s^{-1}, half-barbs = 2.5 m s^{-1}); and bright-band melting level (bold) from the 915-MHz wind profiler at CZD. Hourly averaged surface winds measured at CZD are included. Lower panel: surface traces from CZD (PRS = pressure, T = temperature, T_d = dewpoint, PPT = precipitation) and nearby BBY [PPT (BBY) = precipitation, v_{sfc} = cross-mountain wind component (oriented 50-230 deg)]. The layer-mean hourly consensus cross-mountain wind component measured by the BBY profiler in the lowest 750 m MSL ($v_{0\text{-}750\ m}$) is also shown.

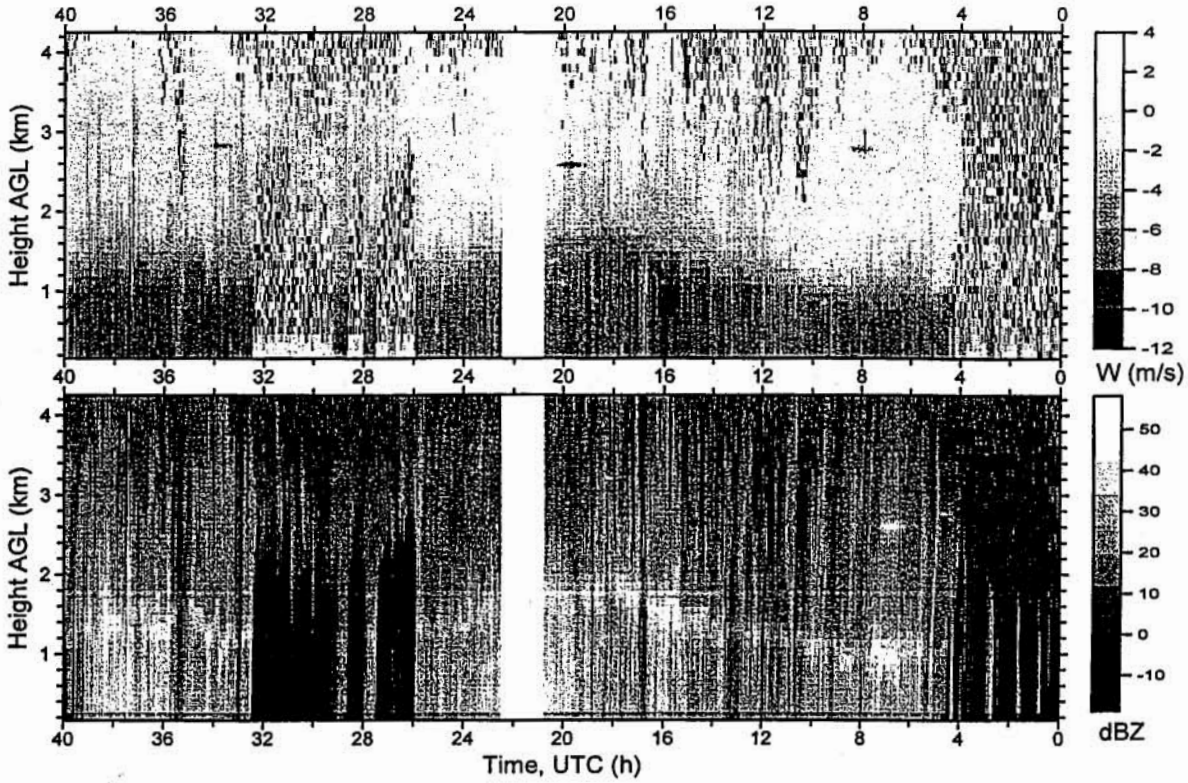

Figure 4. Vertical velocity (top) and radar reflectivity factor (bottom) measured by the S-band radar at CZD. The time axis increases from right to left and begins at 0000 UTC on 5 Feb. The radar was down from 2050-2230 UTC 5 Feb.

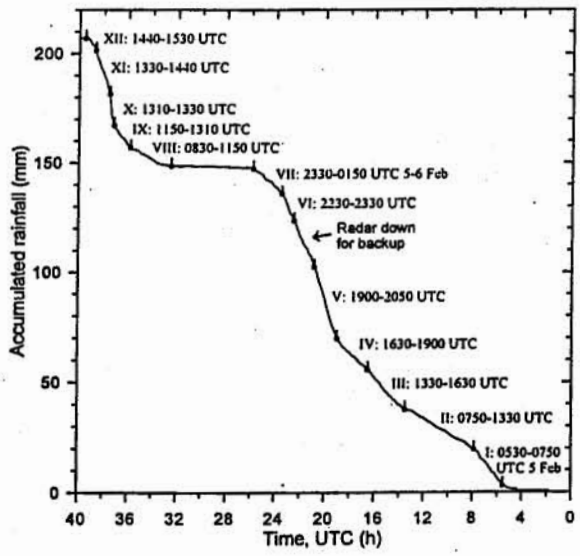

Figure 5. Rainfall accumulation at CZD on 5-6 Feb. The Roman numerals and times denote periods of quasi-steady rainfall rate determined by inspecting time series of fall velocity and dBZ from the S-band radar.

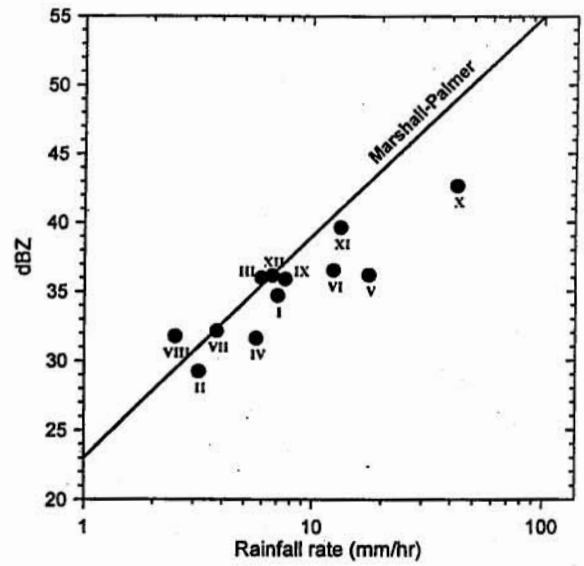

Figure 6. *Z-R* data from CZD for the storm of 5-6 Feb. The reflectivity and rainfall rate data were averaged over the periods defined in Fig. 5. The solid line gives the Marshall-Palmer *Z-R* relationship (see text).